Cell

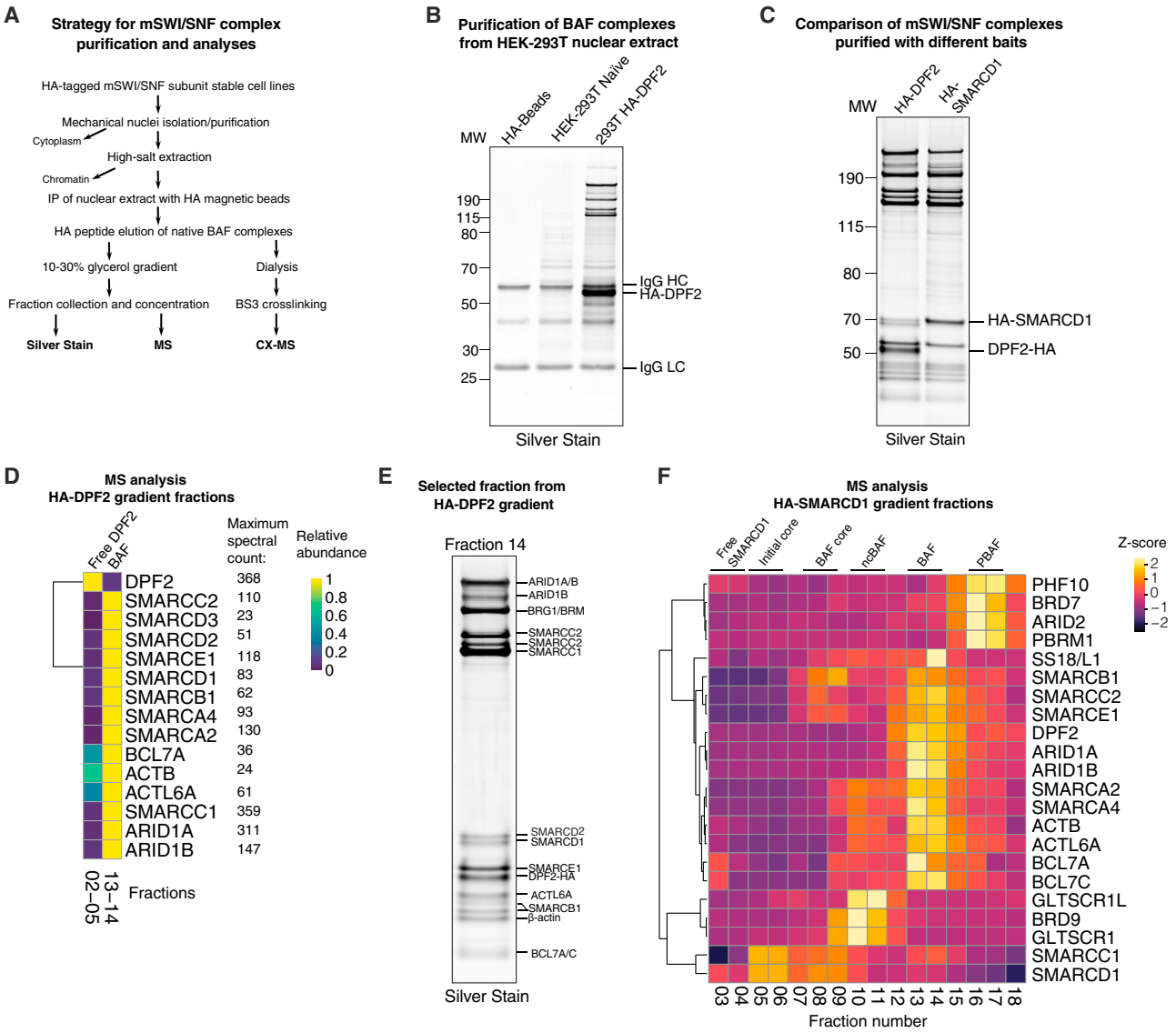

Figure S1. Purification and Gradient Mass Spectrometry of mSWI/SNF Complexes, Related to Figure 1

(A) Schematic of mSWI/SNF complex purification and analyses.

(B) Silver stain of HA bead-bound proteins. HA Dynabeads were incubated with either EB300 (control) or with nuclear extracts from indicated cells, washed, eluted with SDS and loaded onto SDS-PAGE and analyzed using silver staining.

(C) Silver stain of BAF complexes purified using HA-DPF2 or HA-SMARCD1 as baits.

(D) Heatmap clustering of mass-spectrometry-determined peptide abundance on selected fractions collected from HA-DPF2-purified BAF complexes from Figure 1C.

(E) Silver staining of fraction 14 from the HA-DPF2 gradient from Figure 1C. Identified proteins are labeled.

(F) Heatmap clustering of mass-spectrometry-determined peptide abundance across fractions collected from HA-SMARCD1 density gradient in Figure 1B. Color scale reflects z-scores.

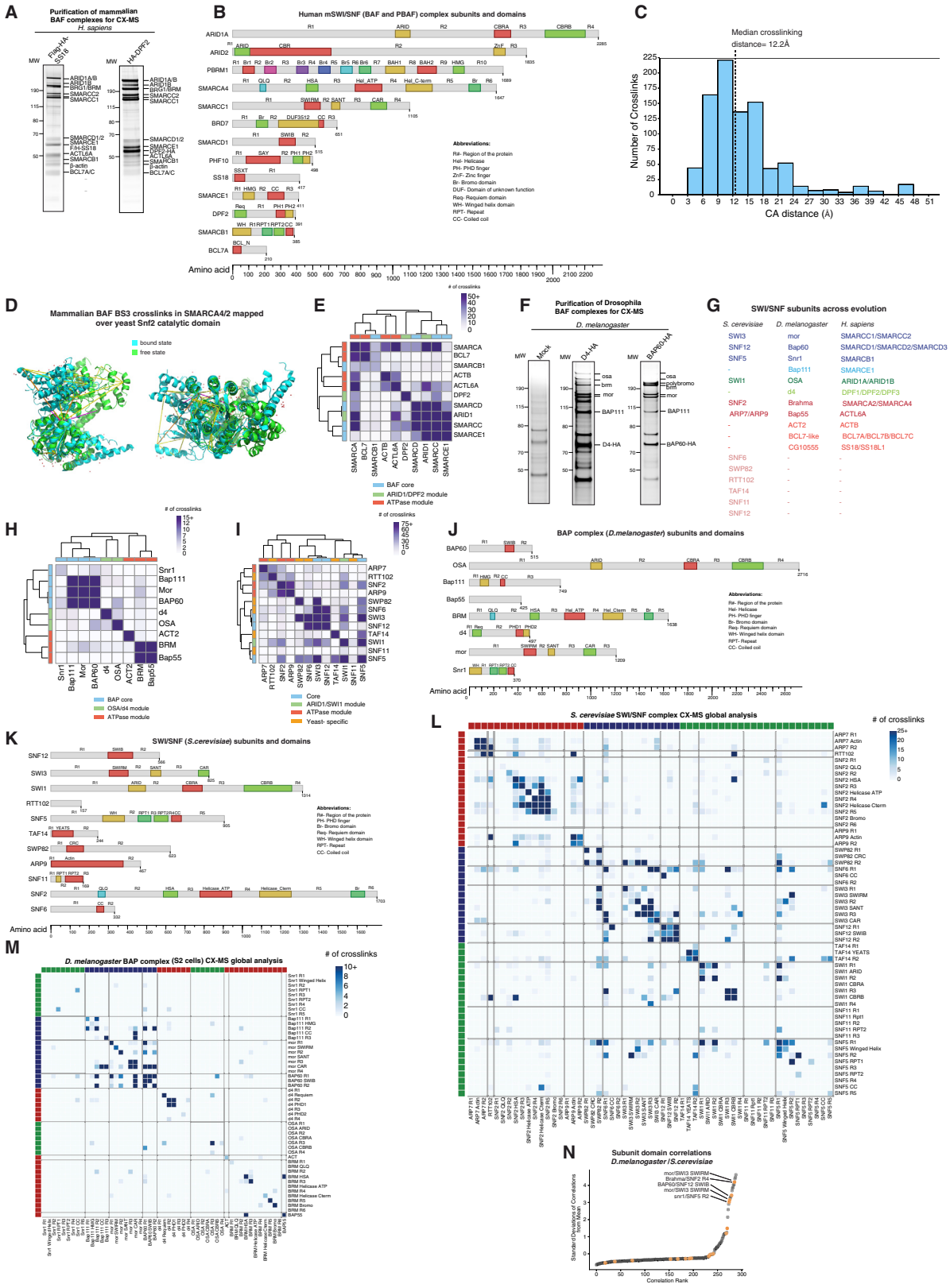

(legend on next page)

Figure S2. Purification and Cross-Linking Mass Spectrometry on Mammalian, Fly, and Yeast SWI/SNF Complexes, Related to Figure 2

(A) Silver stains of affinity-purified complexes from mammalian HEK293T cells expressing Flag-HA-SS18 or HA-DPF2.

(B) Schematic representation of defined and newly-identified regions in mammalian SWI/SNF subunits used in representing inter-subunit crosslinks. Only one paralog of each subunit family is displayed.

(C) Analysis of the distance between crosslinked residues in known 3D structures of mSWI/SNF complex subunit domains. Dashed line indicates the median distance calculated. Length of the BS3 crosslinker spacer is 11.4Å.

(D) Structures of the Snf2 ATPase domain in nucleosome-bound (blue) and nucleosome-free (green) states. SMARCA4 crosslinks in dynamic regions are colored in purple and orange. Crosslinks in constant regions are colored in yellow.

(E) Clustered distribution of the total crosslinks from mammalian BAF complex cross-linking mass spectrometry. Clustering indicates similarly strong correlations between SMARCC, SMARCD, and SMARCE subunits with ARID1, which bridges this module to the ATPases and their associated subunits (See also Figure 2B).

(F) Silver stains of affinity-purified complexes from *D. melanogaster* S2 cells expressing D4-HA, BAP60-HA or mock control.

(G) SWI/SNF subunit orthologs in *S. cerevisiae*, *D. melanogaster* and *H. sapiens*.

(H) Clustered distribution of the total crosslinks from cross-linking mass spectrometry performed on *D. melanogaster* complexes.

(I) Clustered distribution of the total crosslinks from cross-linking mass spectrometry performed on *S. cerevisiae* complexes.

(J) Schematic representation of defined and newly-identified regions in *D. melanogaster* BAP subunits used in representing inter-subunit crosslinks.

(K) Schematic representation of defined and newly-identified regions in *S. cerevisiae* SWI/SNF subunits used in representing inter-subunit crosslinks.

(L) Matrix heatmap of the total crosslinks from *S. cerevisiae* SWI/SNF complex cross-linking mass spectrometry (Sen et al., 2017). Individual subunits are divided into domains (per K) and ordered according to Figure 2D.

(M) Matrix heatmap of the total crosslinks from *D. melanogaster* BAP complex cross-linking mass spectrometry performed as part of this study. Individual subunits are divided into domains (per J) and ordered according to Figure 2C.

(N) Correlation analysis between *D. melanogaster* BAP and *S. cerevisiae* SWI/SNF subunit domain and region interactions from cross-linking mass spectrometry datasets.

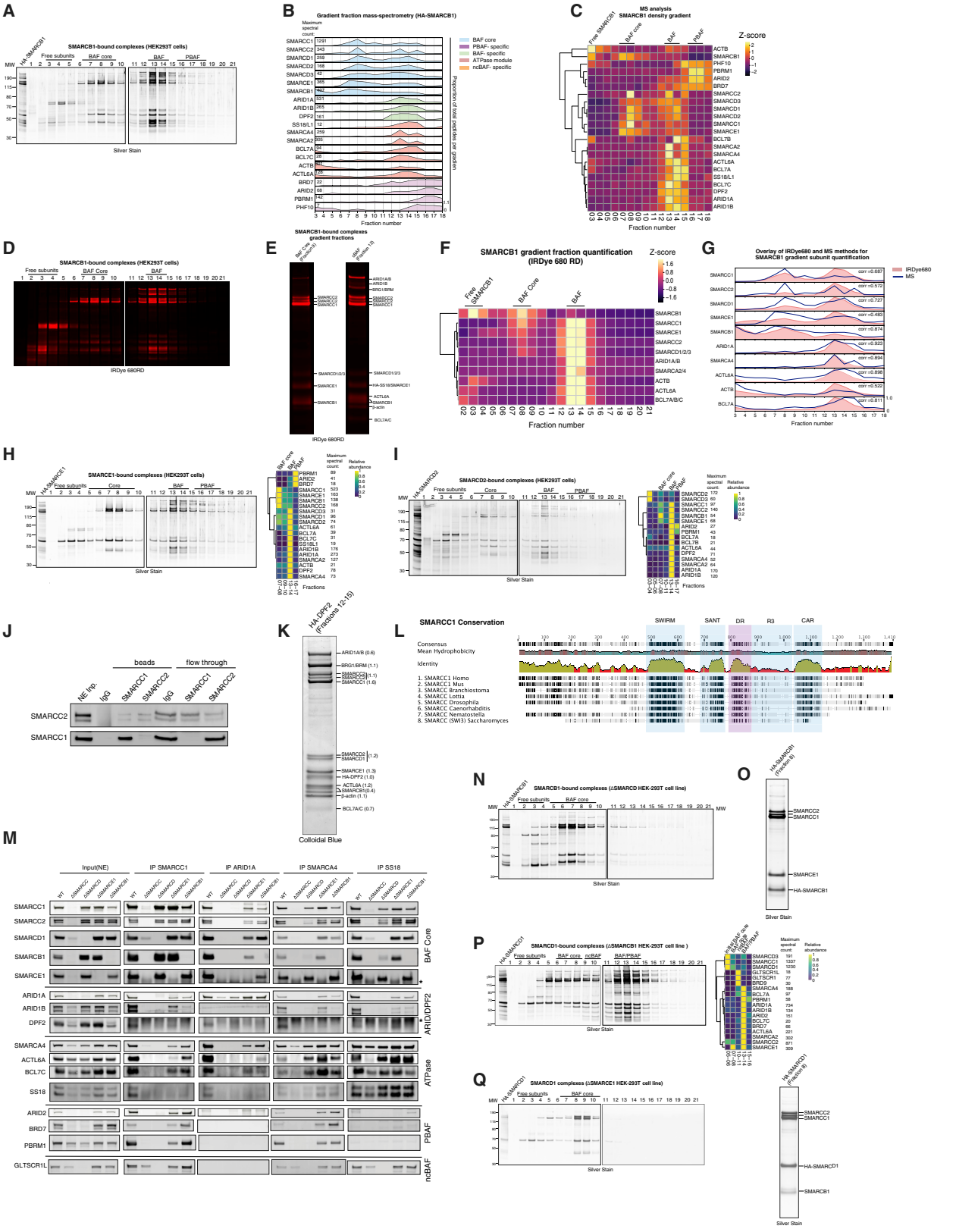

(legend on next page)

Figure S3. Purification and Mass Spectrometry Analyses of the BAF Core Module, Related to Figure 3

(A) Native HA-SMARCB1 BAF complexes purified from WT HEK293T cells and subjected to glycerol gradient centrifugation. Collected fractions were SDS-PAGE separated and silver stained.

(B) Graphical representation of peptide relative abundance in each density gradient fraction identified by mass spectrometry analysis. Total spectral counts from fraction of highest peptide abundance for each subunit are indicated.

(C) Clustering heatmap of HA-SMARCB1 density gradient mass spec fractions displayed as Z-scores.

(D) Native HA-SMARCB1 BAF complexes were prepared as in (A) but each fraction was labeled using IRDye 680RD NHS ester.

(E) IRDye 680RD detection performed on Fractions 9 and 12 from (A). Identified proteins are labeled.

(F) Clustering heatmap of HA-SMARCB1 density gradient IRDye 680RD quantification displayed as a Z-score.

(G) Graphical representation of IRDye 680RD quantification and peptide relative abundance in each density gradient fraction from two independent biological replicates of data displayed in (A) and (D).

(H) Native HA-SMARCE1 BAF complexes purified from WT HEK293T cells and subjected to glycerol gradient centrifugation; collected fractions were SDS-PAGE separated and silver stained (left). Clustering heatmap and spectral counts of HA-SMARCE1 density gradient mass spec fractions (right).

(I) Native HA-SMARCD2 BAF complexes purified from WT HEK293T cells and subjected to glycerol gradient centrifugation; collected fractions were SDS-PAGE separated and silver stained (left). Clustering heatmap and spectral counts of HA-SMARCD2 density gradient mass spec fractions (right).

(J) HEK293T nuclear extracts were immunodepleted using indicated antibodies. Input, IP and flow through fractions were loaded on to SDS-PAGE and analyzed using WB with indicated antibodies.

(K) Representative colloidal blue near infra-red detection of fractions 12-15 from DPF2-purified BAF complexes. Identified proteins are labeled and their approximated stoichiometry relative to DPF2 bait are indicated in parentheses.

(L) Evolutionary conservation of the SMARCC subunits. Conserved domains and regions are indicated.

(M) Co-IP/immunoblot analysis of BAF core module WT and subunit KO cells. Antibodies used for detection are indicated.

(N) Native HA-SMARCB1 BAF complexes were purified from ΔSMARCD 293T cells and subjected to glycerol gradient centrifugation, collected fractions were SDS-PAGE separated and silver stained (left).

(O) Silver stain analysis of Fraction 8 of the HA-SMARCB1 gradient in WT HEK293T cells. Subunits are labeled.

(P) Native HA-SMARCD1 BAF complexes were purified from ΔSMARCB1 cells and were subjected to glycerol gradient centrifugation. Collected fractions were SDS-PAGE separated and silver stained (left). Clustered heatmap and spectral counts of the mass spec analysis performed on selected pulled fractions (right).

(Q) Samples from HA-SMARCD1 gradient in Figure 3G were PAGE-separated and silver stained (short development time).

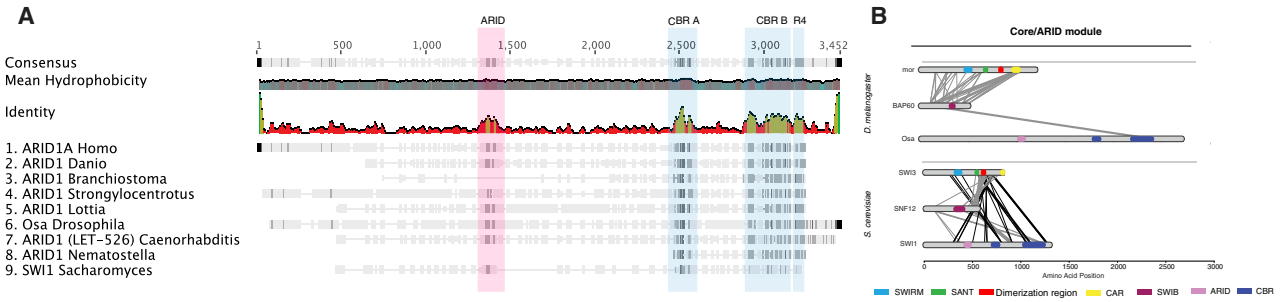

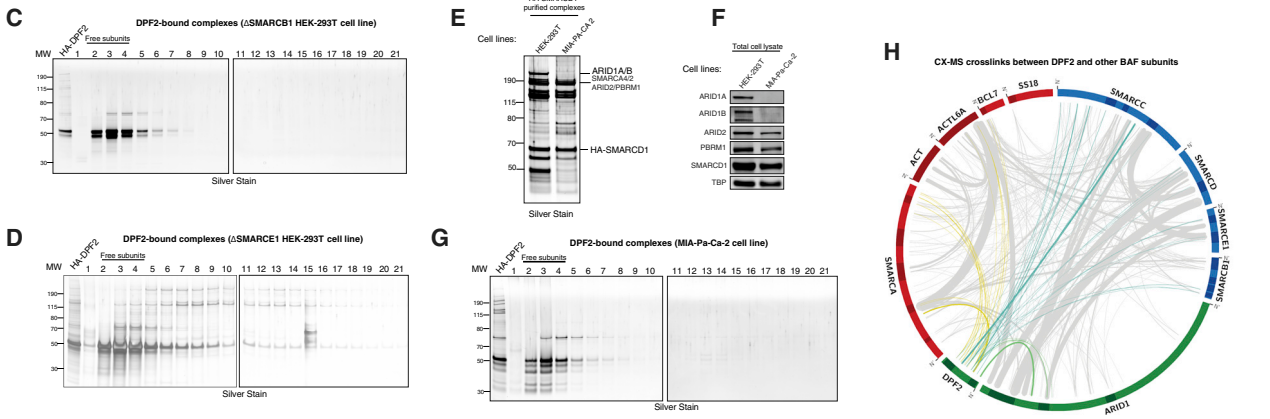

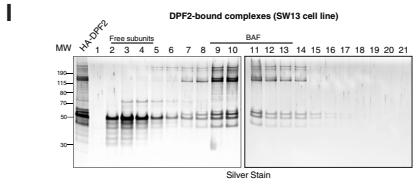

J

MS analysis of DPF2 complexes from SW13 cell line (fractions 9-14)

	Gene Symbol	Unique peptides	Total peptides
	ARID1A	63	125
	ARID1B	45	93
	SMARCC1	43	105
	SMARCC2	33	61
	SMARCE1	24	61
	SMARCD1	22	29
	DPF2	20	61
	SMARCD2	17	29
	SMARCB1	14	28
	SMARCD3	14	19
	ARID2	6	7
	BRD7	2	3
ATPase components	SMARCA4	0	0
ATPase components	SMARCA2	0	0
ATPase components	ACTL6A	0	0
ATPase components	BCL7A	0	0
ATPase components	BCL7B	0	0
ATPase components	BCL7C	0	0
ATPase components	SS18	0	0
ATPase components	SS18L1	0	0
	ACTB	3	3

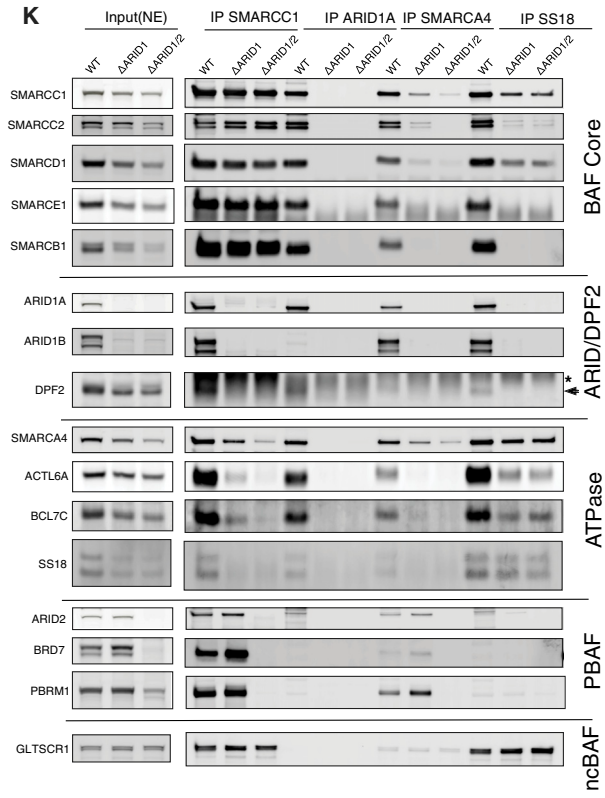

(legend on next page)

Figure S4. Identification and Analysis of the ARID1/DPF Module of mSWI/SNF Complexes, Related to Figure 4

(A) Alignment and conservation analysis of the ARID1 orthologs and identification of the conserved CBR A and CRB B bridging regions.

(B) Crosslinks from orthologous BAF CORE and ARID subcomplexes from *S. cerevisiae* and *D. melanogaster* cross-linking mass spectrometry datasets. Line width is proportional to the number of crosslinks. Black links *in S. cerevisiae* schematic represents crosslinks between SWI3 and SWI1.

(C) Native HA-DPF2 BAF complexes were purified from ΔSMARCB1 cells and were subjected to glycerol gradient centrifugation. Collected fractions were PAGE-separated and silver stained.

(D) Native HA-DPF2 BAF complexes were purified from ΔSMARCE1 cells and were subjected to glycerol gradient centrifugation. Collected fractions were PAGE-separated and silver stained.

(E) Native HA-SMARCD1 complexes were purified from MIA-Pa-Ca 2 cells (ARID1A and ARID1B-dual deficient) and WT HEK293T cells, PAGE-separated and silver stained.

(F) Western blot analysis of the total cell lysates (TCL) from HEK293T and MIA-Pa-Ca 2 cells with indicated antibodies.

(G) HA-DPF2 BAF complexes were purified from MIA-Pa-Ca2 cells and subjected to glycerol gradient centrifugation. Eluted proteins were PAGE-separated and silver stained.

(H) Circle-plot analysis of the mammalian cross-linking mass spectrometry dataset. DPF2 subunits crosslinks to other BAF subunits are indicated. DPF2/ BAF core in teal, DPF2/ARID crosslinks subunits are in green and DPF2/ATPase in yellow.

(I) Native HA-DPF2 BAF complexes were purified from SW13 (SMARCA4/SMARCA2-dual deficient) cells and were subjected to glycerol gradient centrifugation. Collected fractions were separated by SDS-PAGE and silver stained.

(J) Mass spectrometry analysis of the total elution from HA-DPF2 purifications from ATPase-negative SW13 cells.

(K) Nuclear extracts from WT or ARID subunit KO HEK293T cell lines were subjected to immunoprecipitation with indicated antibodies. Eluted samples were PAGE separated and immunoblotted with indicated antibodies.

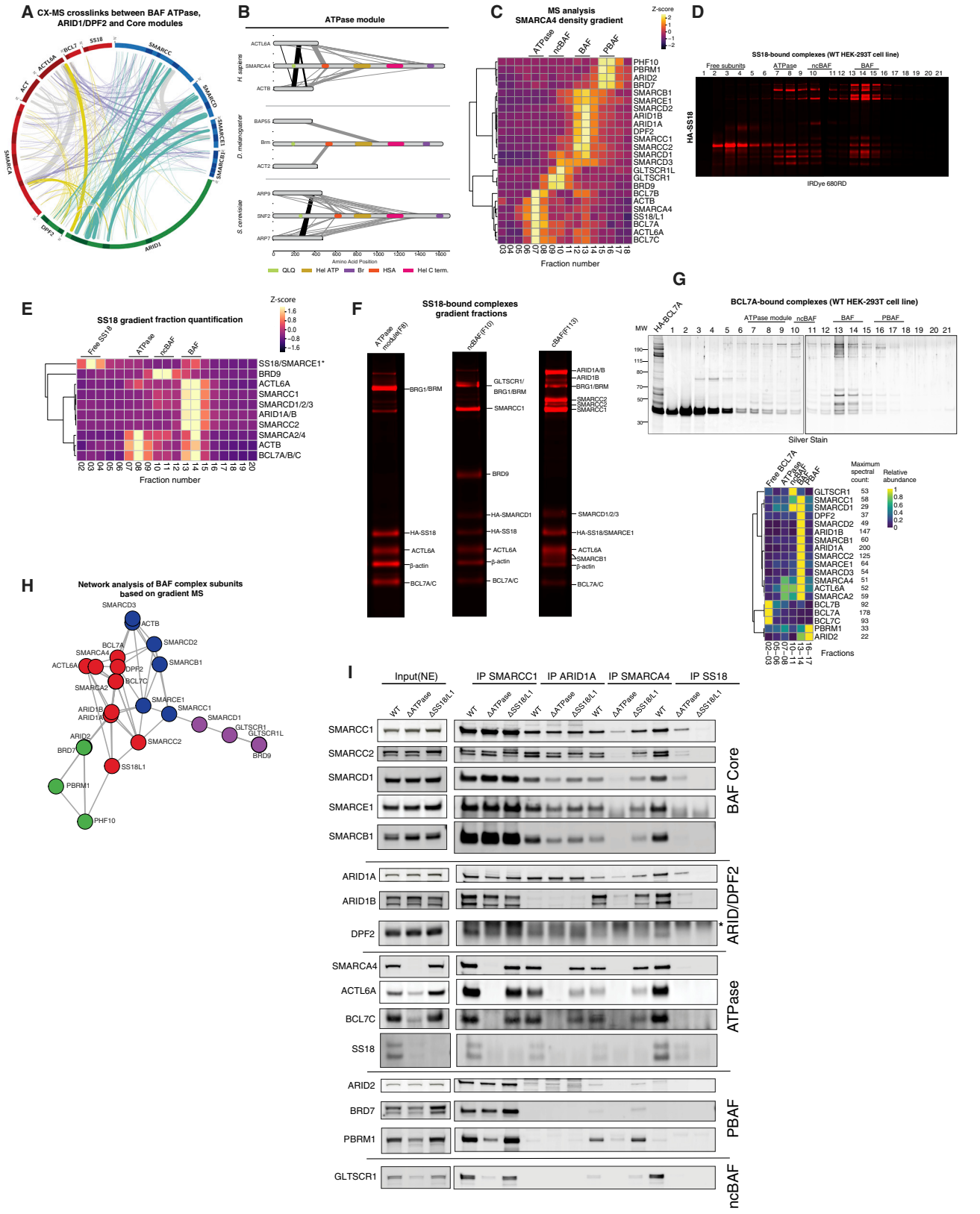

(legend on next page)

Figure S5. Biochemical Purifications and Mass Spectrometry Define the mSWI/SNF ATPase Module, Related to Figure 5

(A) Circle-plot analysis of the mammalian cross-linking mass spectrometry dataset. ATPase/core module subunits crosslinks are in blue, ATPase/ARID module crosslinks are in yellow, and CORE and ARID module subunits are in green. Data from paralogous subunits was combined.

(B) Schematic representation of crosslinks from orthologous ATPase subcomplexes from *H. sapiens*, *D. melanogaster* and *S. cerevisiae* cross-linking mass spectrometry datasets. Line width is proportional to the number of crosslinks. Black lines represent crosslinks between actin-like proteins.

(C) Clustered heatmap of mass spec analysis performed on spectral counts from each fraction collected from HA-SMARCA4 density gradient from WT 293T cells. Colors represent Z-scores, according to legend.

(D) IRDye 680RD detection of fractions from HA-SS18 density gradient from purification in Figure 5E.

(E) Clustering heatmap of HA-SS18 density gradient IRDye 680RD quantification. Colors represent Z-scores according to legend. *= SS18 and SMARCE1 desnities were combined (overlapping sizes).

(F) IRDye 680RD detection performed on Fractions 8, 10 and 13 from (D). Identified proteins are labeled.

(G) HA-BCL7A BAF complexes were purified from WT HEK293T cells and were subjected to glycerol gradient centrifugation. Collected fractions were SDS-PAGE separated and silver stained (left). Clustered heatmap and spectral counts of the mass spec analysis performed on selected pulled fractions (right).

(H) Louvain modularity analysis performed on mass-spec analyses from glycerol gradients collected from SMARCD1, SMARCB1 and SMARCA4 purifications. Colors are generated as a function of the relations between the nodes (subunits) of the generated network.

(I) Nuclear extracts from WT or core BAF subunit KO cell lines were subjected to immunoprecipitation with indicated antibodies. Eluted samples were SDS-PAGE separated and immunoblotted with indicated antibodies.

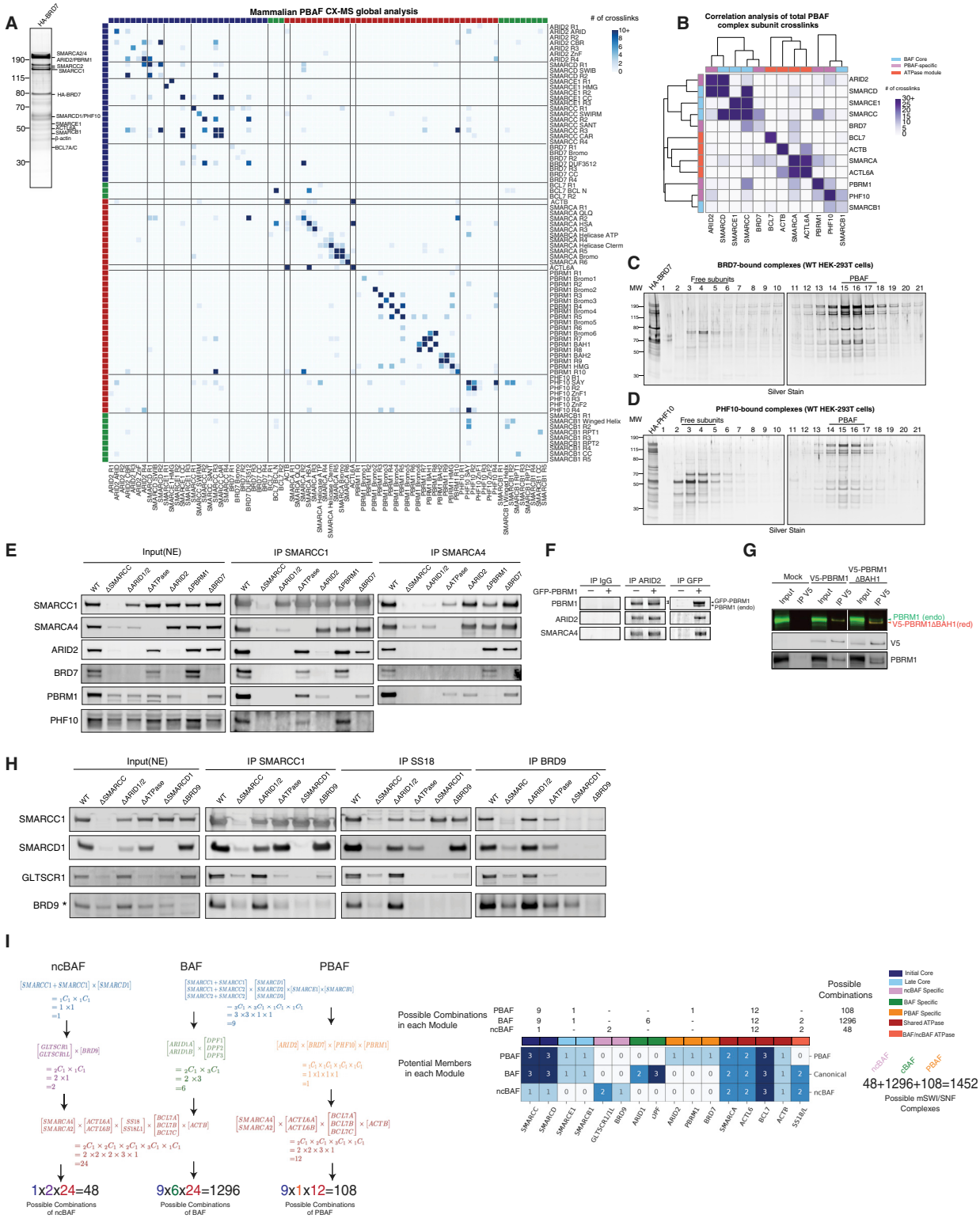

Figure S6. Cross-Linking Mass Spectrometry Analysis of PBAF Complexes, Related to Figure 6

(A) (Left) HA-BRD7 was used as a bait for purification of PBAF complexes for cross-linking mass spectrometry. (Right) Heatmap reflecting distributions of total crosslinks from mammalian PBAF complex cross-linking mass spectrometry. Individual subunits are divided into domains and ordered according to Figure 6C.

(legend continued on next page)

(B) Correlation analysis of the total subunit crosslinks from cross-linking mass spectrometry obtained from PHF10 and BRD7 datasets.
(C) Native HA-BRD7 PBAF complexes were purified from WT HEK293T cells and were subjected to glycerol gradient centrifugation, collected fractions were PAGE separated and silver stained.
(D) Native HA-PHF10 PBAF complexes were purified from WT HEK293T cells and were subjected to glycerol gradient centrifugation, collected fractions were PAGE separated and silver stained.
(E) Immunoblot/co-IP analysis performed on PBAF subunit KO HEK293T cells. Antibodies used for detection are indicated.
(F) HEK293T cells were stably infected with GFP-PBRM1 or empty vector and used for co-IP/immunoblot analyses. Antibodies used for detection are indicated.
(G) HEK293T cells were infected with WT V5-PBRM1, V5-PBRM1ΔBAH1 mutant variant or empty vector and used for WB-co-IP analysis. Antibodies used for detection are as indicated.
(H) WB-co-IP analysis performed on WT and ncBAF subunit KO cells. Antibodies used for detection are indicated. *-Non-specific band above BRD9 band in the input.
(I) Total combinatorial possibilities across mSWI/SNF complex families (including tissue-specific subunits).

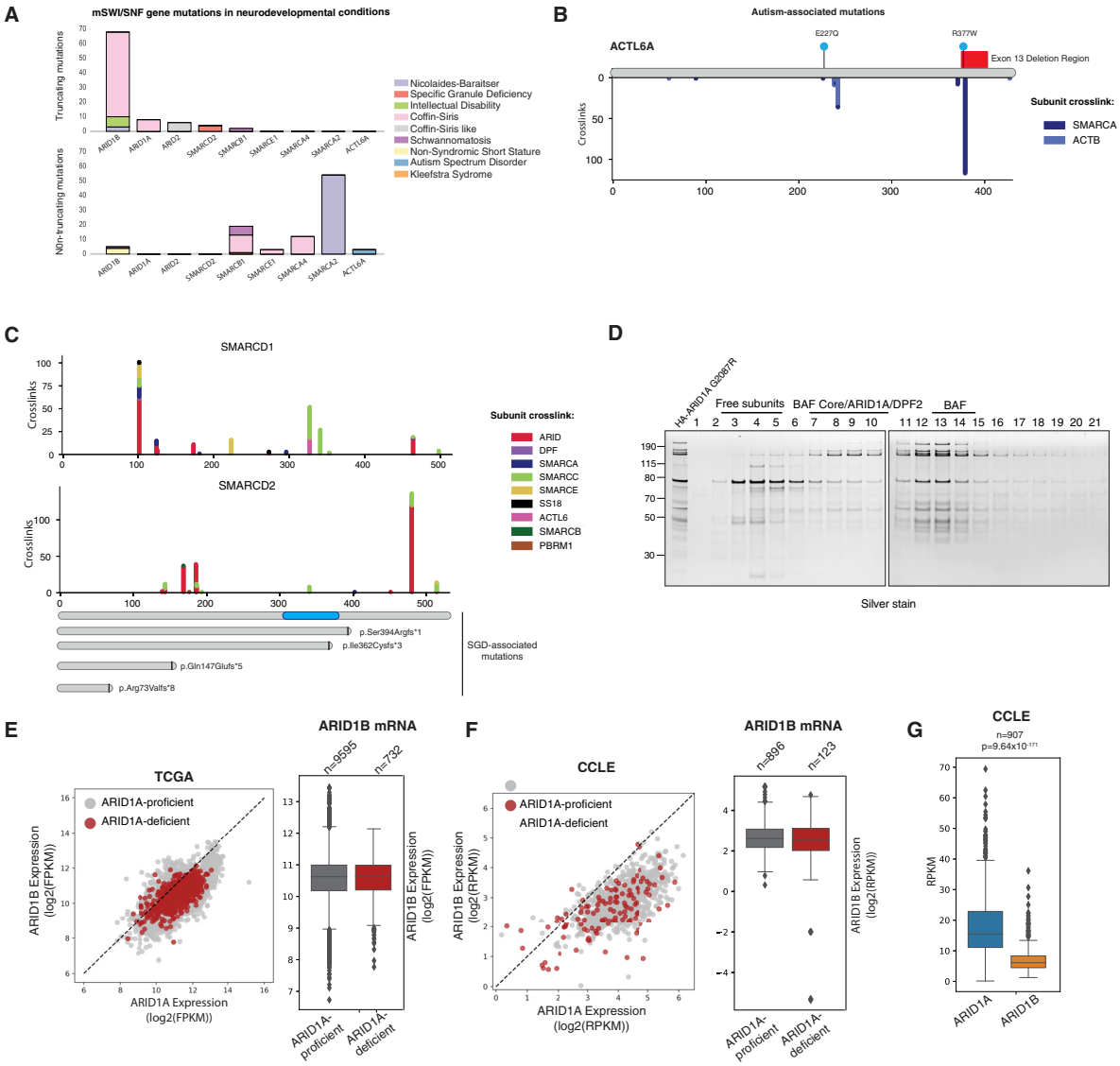

Figure S7. Disease-Associated Perturbations to mSWI/SNF Complex Assembly, Related to Figure 7

(A) Mutations in mSWI/SNF genes in human intellectual disability/developmental syndromes and other diseases.

(B) Mutations in ACTL6A in autism spectrum disorders mapped over crosslinks to the BAF ATPase module.

(C) (Top) Crosslinks in SMARCD1 and SMARCD. (Bottom) mutations in human specific granule deficiency (SGD) and crosslinks to other BAF subunits.

(D) Silver stain analysis performed on glycerol gradient of HA-ARID1A G2087R-purified BAF complexes from HEK293T cells.

(E) mRNA expression levels of the ARID1A and ARID1B transcripts in ARID1A-proficient and -deficient cancers (left). Boxplot of ARID1B expression in ARID1A-proficient and -deficient cancers (right).

(F) mRNA expression levels of the ARID1A and ARID1B transcripts in ARID1A-proficient and -deficient CCLE cancer cell lines (left). Boxplot of ARID1B expression in ARID1A-proficient and -deficient CCLE cell lines (right).

(G) Boxplot of expression of ARID1A and ARID1B across CCLE cell lines. All represented cell lines have WT ARID1A and ARID1B.